Understanding the Mechanism of CO_2 to CO Conversion by Ruthenium Polypyridyl Catalysts

Xiaoyu Chen[a], Ben A. Johnson[b], Sacha Ott[b], Mårten S. G. Ahlquist[a*]

[a] Department of Theoretical Chemistry & Biology, School of Engineering Sciences in Chemistry, Biotechnology and Health, KTH Royal Institute of Technology, 10691-Stockholm, Sweden

[b] Department of Chemistry, Ångström Laboratory, Uppsala University, Box 523, 751 20 Uppsala, Sweden

Carbon Dioxide Reduction • Electrocatalysis • Ruthenium Polypyridyl • DFT • Mechanism

ABSTRACT: A detailed mechanistic study of ruthenium 2,2′:6′,2′′-terpyridine (tpy) 2,2′-bipyridine (bpy) class of catalysts is presented, with all three key stages (i.e. solvent dissociation, C-O bond cleavage and CO dissociation) discussed. DFT calculations together with kinetic studies revealed that the introduction of a methyl substituent on the bipyridine ligand eases solvent dissociation and hence allow catalysis to take place at the first reduction potential as the five coordinated Ru complex is easier to reduce. This highlights the importance of steric effect in catalyst-design. For C-O bond cleavage, DFT calculations suggest that proton acts as a much better oxide accepter compared to CO_2, explaining the improved activity when water is added to the system. To further understand how the electronic nature of the ring substitutes affects the reactivity, we designed a hypothetical catalyst with fluorine substitutes and found out electron withdrawing groups lower the reductive potentials at a cost of harder solvent dissociation. For the final CO dissociation, due to the special nature of carbonyl ligands, neither steric nor electronic alternations can ease the step and here is where *kinetic trans effect* comes into play. In line with a recent experimental work, our DFT calculations showed that when a carbene group is trans to CO, the dissociation rate is increased dramatically.

The dramatic increase in human activity, especially the burning of fossil fuels, in the last few decades has caused a raise change in atmospheric CO_2 concentration[1,2] . In nature, CO_2 is reduced by green plants and photosynthetic bacteria, which has inspired researchers to develop artificial strategies that can perform the same overall reaction in a controllable manner[2]. Specifically, recent research on CO_2 reduction focused on the reduction of CO_2 to: 1) carbon monoxide[3]; 2) formic acid[4]; 3) formaldehyde[5]; 3) methanol[6]; 4) longer chain hydrocarbons[7] and 5) other reduced form of carbon[8]. It is believed that recycling of CO_2 can be a potential long-term solution to global warming and even the global energy crisis.

At very high temperatures, certain transition metal oxides, such as CeO_2, ZnO_2 or FeO_2, can reduce CO_2 to produce carbon monoxide[9]. Although these thermochemical conversions are associated with higher rate constants than the photo- or electrocatalytic reductions, the equipment are expensive, which may be a limiting factor for large scale industrial applications. As first introduced by Honda and co-workers[10] in 1979, CO_2 can also be reduced photoelectrochemically to formaldehyde or methanol by semiconductors such as TiO_2[11], ZnO/Cu[12], and CdS[13]. In these systems, CO_2 is reduced by the photo-excited electrons in the conduction bands. However, the band gaps of these simple metal oxides do not match well the reduction potential of CO_2, resulting in a low overall efficiency. Although the bandgaps can be adjusted by processes such as doping, the ideal candidate has not yet been found.

Another strategy to reduce CO_2 is via electrochemistry. It is possible to use electrical energy generated from a renewable source making the whole process more sustainable. Thermodynamically, the standard reductive potential required to reduce CO_2 to CO is -1.28V (vs. $Fc^{+/0}$) in CH_3CN[14] and -0.53V (vs. SHE) in water. One advantage of conducting experiments in aprotic solvent is that proton reduction, which competes with the proton assisted CO_2 reduction, is completely eliminated. Moreover, CO_2 dissolves better in organic solvents compared to in water. To be specific, its solubility in acetonitrile[15] is about 0.279 mol/L while it is only 0.033mol/L in water. As a result, several metal complexes that are inactive under aqueous conditions show some reactivity in organic solvents[15].

$$2H^+ + 2e^- \longrightarrow H_2 \qquad E^o = 0.00\ V \quad vs.\ SHE$$
$$CO_2 + 2H^+ + 2e^- \longrightarrow CO + H_2O \qquad E^o = -0.53\ V \quad vs.\ SHE$$
$$2\ CO_2 + 2e^- \longrightarrow CO + CO_3^{2-} \qquad E^o = -1.28\ V^{14} \quad vs.\ Fc^{+/0}$$

One major concern in electrochemical CO_2 reduction is that one-electron reduction yields the highly energetic CO_2^- radical (-1.90V vs. SHE). In order to avoid this intermediate, and thereby lower the high reductive potential associated with the direct reduction of CO_2, one strategy is to build multiple reductive equivalents at the catalyst site, which can then act as a multiple electron reservoir[8].

$$CO_2 + e^- \longrightarrow CO_2^- \qquad E^o = -1.90\ V \quad vs.\ Fc^{+/0}$$

In aprotic, homogeneous systems, metal porphyrins[16], for example tetraphenylporphyrin (TPP)[17], Re(bpy)(CO_3) [18] as well as many other species have been reported for their promising electrocatalytic properties. In heterogeneous systems, examples include transition metal catalysts such as Ni(cyclam) [19] Mn(bpy)$(CO)_3$ [20], and Re(bpy)$(CO)_3$ [21].

Among many transition metal based catalysts, a class of Ru(tpy)(bpy) catalysts is particularly interesting since they are relatively easy to tune electronically and sterically by ligand modification[22]. For molecular catalysts, a minimal change in structure molecular catalysts can sometimes lead to significant improvements in their reactivities[23-25]. Until recently, it was generally accepted that an initial two-fold reduction is required to active this type of catalyst. In 2016, S.Ott and co-workers[26] reported that the introduction of a methyl substituent on the bipyridine ligand (Catalyst **B**, Figure 1) can lower the over-potential significantly by triggering electrocatalysis at the first reduction potential, which was not known previously.

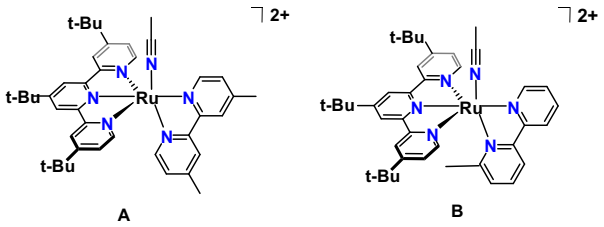

Figure 1. The geometries of Catalyst A^{2+} and B^{2+} involved in this study

Results and Discussions

In electrochemistry, efficiency is linked to over-potential, which is defined as the difference between the potential at which the electrochemical reaction is observed and the thermodynamic reductive potential of the reaction. Based on this definition, the over-potential for catalyst **B** is only -0.48V (-1.76V – (-1.28V) = -0.48V), which is much lower than what was observed for catalyst A (-2.09V – (-1.28V) = -0.81V). However, we should also note that although catalyst **B** shows some activity at the first reduction potential, the maximum catalytic current is not achieved until the applied potential reaches ca. -2.4 V, which is about the same as for catalyst **A**.

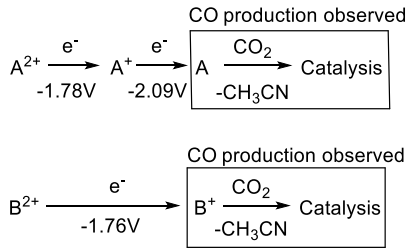

Scheme 1. The activation of the two catalysts

Catalyst Activation

The dissociation of CH_3CN is crucial for catalyst activation as it provides a vacant site for CO_2 binding. In general, it takes place after the second reduction for $[Ru(tpy)(bpy)]^{2+}$ type of catalysts. What is special about catalyst **B** is that this step can take place after only one reduction thanks to the steric hindrance provided by the bpy methyl, which in turn, weakens the CH_3CN-catalyst interaction through non-optimal orbital overlap.

According to our calculations, the Ru-CH_3CN bond strength is 25.1 kcal/mol for Cat.$\mathbf{A}^+$ but merely 4.5 kcal/mol for Cat.$\mathbf{B}^+$, which is even lower than the binding energy for the twice reduced Cat.$\mathbf{A}^0$ (9.5 kcal/mol). For Cat.$\mathbf{B}^0$, CH_3CN dissociation is exergonic with a free energy change -7.4 kcal/mol, which explains why the second reduction is always irreversible in the cyclic voltammetry (CV) even at faster scan rates[26]. Both bonding energy calculations and the CV data indicate that CH_3CN does not bind as strong with catalyst B as compared to with catalyst **A**. Moreover, it was observed experimentally that when the scan rate is very slow (25 mV s^{-1}), even the first reduction peak becomes irreversible[26] in the case of catalyst **B**, indicating that the dissociation of CH_3CN can take place after only one reduction.

Two possible reaction pathways are presented in Scheme 2. Our calculations suggest that a second reduction is required otherwise the system has to overcome a high energy $[Cat.\ B^+ \cdots CO_2]^{\ddagger}$ transition state. Apart from a facile and rapid CH_3CN dissociation kinetics, in order for catalysis to take place at the first reduction potential, the uptake of a second electron has to proceed at a reductive potential that is not more negative. Kinetic studies have suggested that $Cat.B^+$ undergoes disproportionation to afford $Cat.B^0$, which can then bind with CO_2 easily.

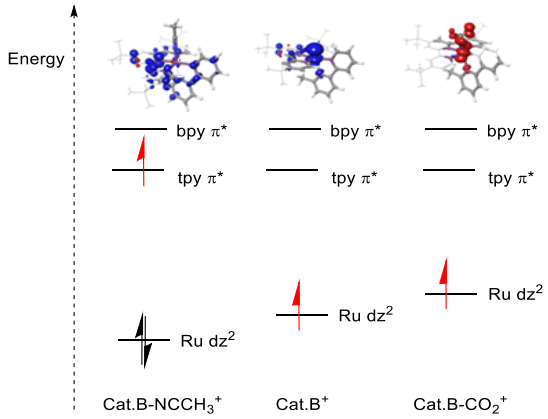

Figure 2. The frontier orbital occupation of catalyst B through the activation stage

Spin density analysis confirmed that the first reduction is tpy based. Since CH_3CN bonds through donating its nitrogen lone pair to ruthenium's d_z^2 orbital, after its dissociation, the previously occupied, lower lying, Ru d_z^2 orbital is now accessible. As CH_3CN dissociation takes place, the injected electron moves from the higher lying tpy π* orbital to the lower lying Ru dz^2 orbital, which significantly lowered the partial charge on Ru centre and hence facilitates CO_2 binding (Figure 2).

Electrocatalysis

In the absence of a proton source, another molecule of CO_2 acts as the oxide acceptor to assist C-O bond cleavage,

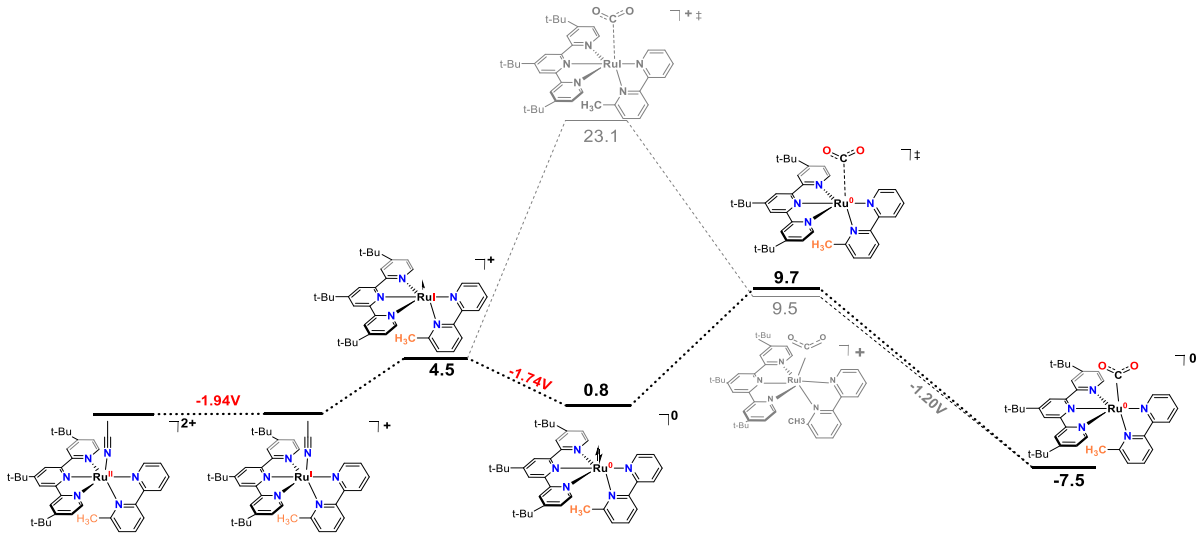

Scheme 2. The activation of catalyst B at the first reduction potential (-1.94V)

releases CO_3^{2-} and CO subsequently to close the catalytic cycle. The relevant Gibbs free energies as well as reductive potentials are calculated by DFT and are presented in Scheme 5.

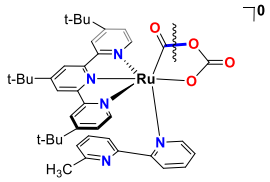

Figure 3. The structure of cyclic [Cat.B-$COOCO_2$]^{c,0}, with the to-be-broken C-O bond highlighted in blue

However, C-O bond cleavage is very difficult ($\Delta G^{\neq}$=60.5 kcal/mol, Scheme 3), if not impossible, at the first reduction potential (-1.94V). In our previous work (Paper II), we proposed a new reaction mechanism via a cyclic [Cat.**B**-$COOCO_2$]^{c,0} intermediate (Figure 3): The flexibility of the tpy framework allows one Ru-N bond to dissociate and hence allows a terminal oxygen in [Cat.**B**-$COOCO_2$]^0 to bind with the ruthenium centre, which acts as an acid to weaken the C-O bond of interest. As a result, the activation free energy for C-O bond cleavage is lowered from 60.5 kcal/mol to merely 10.3 kcal/mol. Thereafter, the complex undergoes one further reaction (-1.78V) and then releases CO_3^{2-} to afford Cat.**B**-CO^+ (Scheme S2). This mechanism is associated with an activation free energy of 20.0 kcal/mol, which is in good agreement with the experimental rate constant.

The 2001cm^{-1}, 1959cm^{-1} and 1933 cm^{-1} peaks from the experimental IR (Figure S1) are assigned to Cat.**B**-CO^{2+} (calc. 2003cm^{-1}, Figure S2), Cat.B-CO^+(calc. 1951cm^{-1}, Figure S3) and Cat.B-CO^0(calc. 1919cm^{-1}, Figure S4) respectively according to our calculations, suggesting that Cat.**B**-CO^+ undergoes a disproportionation reaction to afford Cat.**B**-CO^{2+} and Cat.B-CO^0, while Cat.**B**-CO^{2+} can be reduced to Cat.B-CO^0 without difficulty (Scheme 3), note that the first reduction has a strong driving force at -1.94V. This mechanism also explains why a decrease in Cat.**B**-CO^{2+} concentration was observed after an initial increase in IR (Figure S1) as time goes by.

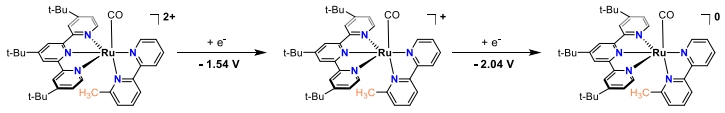

Scheme 3. The subsequent reductions of the Cat.B-CO^{2+}

It is also worth noting that there is not much difference in the energy profiles for the two catalysts should the classical CO_3^{2-} dissociation mechanism (Scheme S1) be followed. This is understandable as the binding of the second CO_2 as well as subsequent reactions happen further away from both the ruthenium centre and the bipyridine-methyl, hence the nature of the latter does not interfere much with the reaction mechanism. For catalyst **A**, since a second reduction is required before the release of CH_3CN, it is not possible to form the Cat.**A**-CO_2^0 complex at the first reduction potential. Therefore, no catalysis was observed at this reductive potential.

Proton as Oxide Acceptor

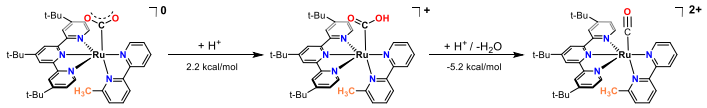

Scheme 4. The energy profile at the first reduction potential at a proton concentration of 10^{-14} M

In the presence of a proton source, usually by adding phenol or water to the system, it can act as the oxide acceptor. Our

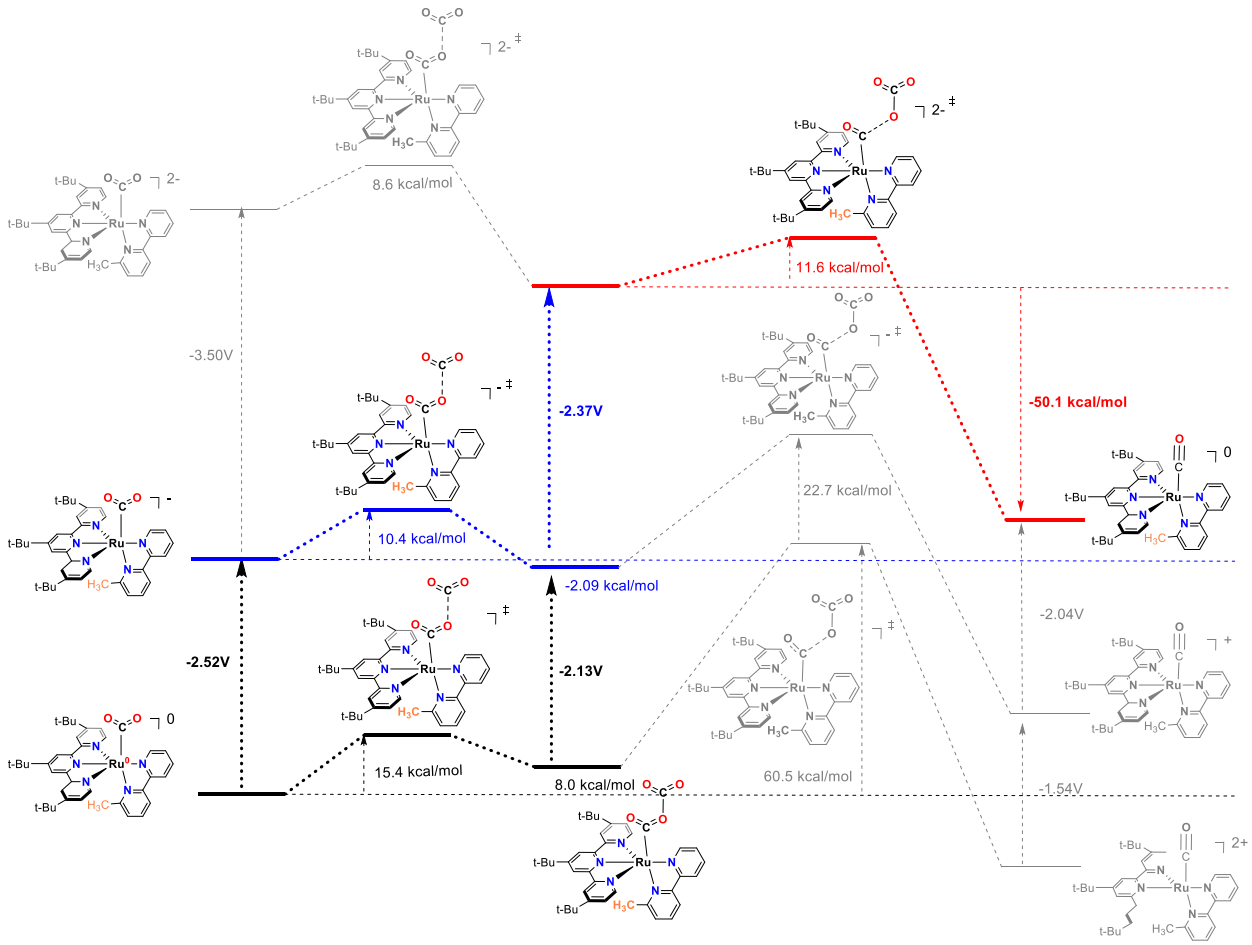

Scheme 5. The possible reaction pathways at different oxidation states for Cat.B-CO_2

calculations suggest that even at very low proton concentration (pH=14), C-O cleavage can still take place much easier (Scheme 4). This is in line with experimental observations – when water was added to the system, the catalytic current was greatly enhanced. In specific, when water concentration was 5.1M, the catalytic current was tripled. However, one should bear in mind that proton reduction acts as a competing reaction and also too much water can change the polarity of reaction medium significantly hence reduce the solubility of the catalyst.

Structural Modification

An earlier work also by Ott and co-workers[25] illustrated that the reductive potentials for Ru(tpy)(bpy) type of catalysts became less negative when the bpy ligand was modified with electron-withdrawing groups due to their strong electron accepting ability. If the ligands are modified with better electron withdrawing groups, then not only the first two, but also the subsequent reductions could become easier resulting in a lowered over-potential for catalysis. This is true to some extent, however, the reactivity for such catalysts are worse in terms of turn over frequency (TOF). Hereby we present a hypothetical catalyst **C**, which consists of a strong electron withdrawing tpy ring modified by fluorine substitutes and a 6-mbpy ring that can weaken the Ru-$NCCH_3$ interaction through steric hindrance as previously discussed.

The calculated reductive potentials are -1.44V and -1.50V respectively (Scheme 6) providing an ECE mechanism (electrochemical, chemical, electrochemical) is followed. However, while the reductions are indeed easier, the catalyst–CH_3CN interaction becomes stronger as a direct result of a relatively electron-poor metal center. Although CH_3CN dissociation is still possible after only one reduction (13.5 kcal/mol as compared to barely 4.5 kcal/mol for the Cat.B-$NCCH_3$ complex), the once reduced catalyst C is not electronegative enough to interact with CO_2. Furthermore, the twice reduced Cat.**C**-CO_2^0 complex is again not reactive enough to bond with another CO_2, without further reductions.

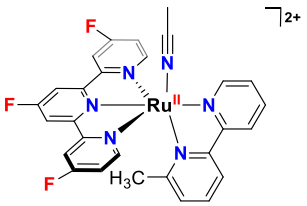

Figure 4. The structure of catalyst **C**

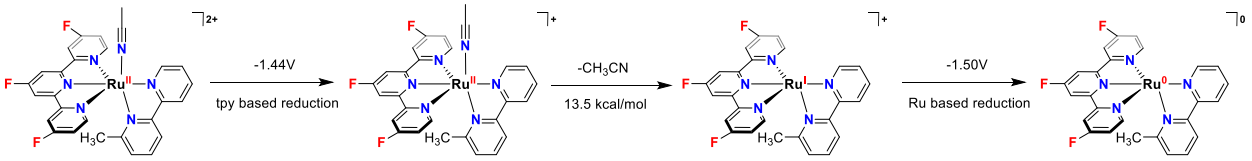

Scheme 6. The activation of the hypothetical catalyst **C**

In summary, although the reductions can be made easier though the introduction of electron-withdrawing groups, the chemical reactions (i.e. CH_3CN dissociation and CO_2 binding) in turn become more difficult. Therefore, despite the fact that catalysis may be observed at a lower reductive potential, the rate is also significantly lowered as a result of the harder chemical reactions.

CO Dissociation

The final step, CO dissociation have with very similar free energy changes for catalyst A, B and C (15.6 kcal/mol, 15.9 kcal/mol and 16.1 kcal/mol respectively). In order to deepen our understanding, we calculated the dissociation free energy for the 2+, 1+ and neutral states for all three catalysts.

	2+ state	1+ state	Neutral
Catalyst A	42.8	35.1	15.6
Catalyst B	33.4	15.8	15.9
Catalyst C	41.3	23.1	16.1

Table 1. CO dissociation energy at varies oxidation state (unit: kcal/mol)

The Ru-CO bond consists of two components: 1) σ donation from the lone pair on carbon to a vacant metal d-orbital; 2) A filled metal d-orbital interact with the empty π* orbital of CO to compensate the increase in electron density through a so-called π-backbonding. Although σ bonding is weakened through reductions, π-backbonding is strengthened due to the increased electron density at the metal center. The strengthened π-backbonding weakens and enlongates C-O bond as the system becomes more reduced (2+ state: 1.15Å. 1+ state: 1.16Å, neutral state 1.17Å for all three catalysts).

Therefore, if we compare CO dissociation and CH_3CN dissociation that we discussed earlier, we can notice that the latter (a pure σ bond) is weakened significantly for both catalyst **A** and **B** through reductions (Table 2).

	2+ state	**1+ state**	**Neutral state**
Catalyst A	41.0	25.1	9.5
Catalyst B	27.0	4.5	-7.4

Table 2. CH3CN dissociation free energy (unit: kcal/mol) for Catalyst **A** and **B**

For catalyst B, a worse orbital overlap caused by the steric effect produced bpy methyl leads to a lower dissociation energy at the +2 and +1 oxidation states compared to catalyst A. As for catalyst B and C, the only difference is that catalyst C has an electron deficient tpy ring, which results in a relatively lowered electron density at the Ru center at the same oxidation state and hence significantly strengthened the sigma donation portion of the Ru-CO bond, and hence larger dissociation free energy.

However, when Cat.B-CO^+ is reduced to Cat.B-CO^0, the strengthened π-backbonding compensates the weakened σ bond and results in the negligible change in CO dissociation free energy. It can be rate-limiting under main catalysis (Scheme 3) as compared to the free energy changes of the previous steps, at an applied potential of ca. -2.5V. That is, all the modifications we have discussed so far have little effect on the free energy required for this final step. However, we have not yet altered the electronic nature of the bidentate ligand much.

A recent study by J.M. Miller and co-workers[27] illustrated that for a Ru(tpy)(pyridyl-carbene) catalyst, where CO can bond *trans* to either the pyridine (N-Ru-CO) or the carbene (C-Ru-CO) site. Significant improvement in CO dissociation rate was observed for the C-Ru-N isomer experimentally (Scheme 7).

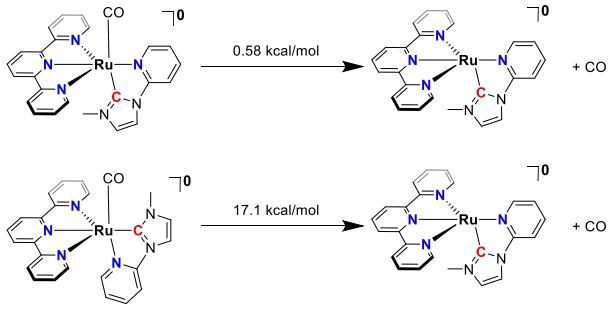

Scheme 7. Calculated CO dissociation energy for different Ru(tpy)(pyridyl-carbene) isomers: C-Ru-CO (up) and N-Ru-CO (down)

Conclusion

Through DFT calculations we demonstrated that the steric hindrance introduced by the bpy-methyl weakens the Ru-$NCCH_3$ bond and hence allows acetonitrile dissociation to take place after only one reduction, which in turn, enables a previously not accessible catalytic pathway without further reductions via a cyclic [Cat.**B**-$COOCO_2$]^{c,0} intermediate. At more negative applied potential, the mechanism, as well as activation energies are very similar for both catalyst **A** and

B, indicating that the effect of bpy-methyl remains local while catalysis can occur further away from the metal centre.

Furthermore, our calculations confirmed that water is a superb oxide acceptor compared to CO_2. In the presence of water, the free energy required for C-O bond cleavage is significantly reduced. However, the final CO dissociation is relatively unaffected by many steric and electronic alterations. In line with a recent work[27] on the *trans effect* in electrocatalytic CO_2 reduction, our work explained the improved reactivity caused by a *trans* carbene group and hence offered a sound design principle for this type of catalysts.

AUTHOR INFORMATION

Corresponding Author

*ahlqui@kth.se

Author Contributions

The manuscript was written through contributions of all authors. All authors have given approval to the final version of the manuscript.

Funding Sources

MA has been supported by the Swedish Research Council (VR) and the Knut & Alice Wallenberg (KAW) project CATSS. XC acknowledges the China Scholarship Council CSC for financial support.

Notes

The authors declare no competing financial interest.

ACKNOWLEDGMENT

The computations were enabled by resources provided by the Swedish National Infrastructure for Computing (SNIC), which is funded by the Swedish Research Council through grant agreement no. 2016-07213, in Linköping (NSC) under project number SNIC 2016/1-19, 2017/1-13, 2019/3-6 and 2020/5-41. We acknowledge NordForsk (No. 85378) for the Nordic University hub NordCO₂. MA has been supported by the Swedish Research Council (VR) grant number 2018-05396, and the Knut & Alice Wallenberg (KAW) project CATSS (KAW 2016.0072). XC acknowledges the China Scholarship Council CSC for financial support.

ASSOCIATED CONTENT

Supporting Information

The Supporting Information is available free of charge on the ACS Publications website.

Methodology, the reaction profile for catalyst **A** and the DFT calculated IRs (file type, PDF)

The xyz coordinates of optimised structures (filetype, PDF)

REFERENCES

(1) Pachauri, R. K.; Allen, M. R.; Barros, V. R.; Broome, J.; Cramer, W.; Christ, R.; Church, J. A.; Clarke, L.; Dahe, Q.; Dasgupta, P.; Dubash, N. K.; Edenhofer, O.; Elgizouli, I.; Field, C. B.; Forster, P.; Friedlingstein, P.; Fuglestvedt, J.; Gomez-Echeverri, L.; Hallegatte, S.; Hegerl, G.; Howden, M.; Jiang, K.; Jimenez Cisneroz, B.; Kattsov, V.; Lee, H.; Mach, K. J.; Marotzke, J.; Mastrandrea, M. D.; Meyer, L.; Minx, J.; Mulugetta, Y.; O'Brien, K.; Oppenheimer, M.; Pereira, J. J.; Pichs-Madruga, R.; Plattner, G. K.; Pörtner, H. O.; Power, S. B.; Preston, B.; Ravindranath, N. H.; Reisinger, A.; Riahi, K.; Rusticucci, M.; Scholes, R.; Seyboth, K.; Sokona, Y.; Stavins, R.; Stocker, T. F.; Tschakert, P.; van Vuuren, D.; van Ypserle, J. P., *Climate Change 2014: Sythesis Report. Contribution of Work Groups I, II and III to the Fifth Assessment report of the Intergovernmental Panel on Climate Change*. IPCC: Geneva, Switzerland, 2014; p 151.

(2) Treadway, J. A.; Moss, J. A.; Meyer, T. J., Visible region photooxidation on TiO2 with a chromophore- catalyst molecular assembly. *Inorg. Chem* **1999,** *38* (20), 4386-4387.

(3) Hansen, H. A.; Varley, J. B.; Peterson, A. A.; Nørskov, J. K., Understanding trends in the electrocatalytic activity of metals and enzymes for CO2 reduction to CO. *J. Phys. Chem. Lett.* **2013,** *4* (3), 388-392.

(4) Kortlever, R.; Peters, I.; Koper, S.; Koper, M. T., Electrochemical CO2 reduction to formic acid at low overpotential and with high faradaic efficiency on carbon-supported bimetallic Pd-Pt nanoparticles. *ACS. Catal.* **2015,** *5* (7), 3916-3923.

(5) Nakata, K.; Ozaki, T.; Terashima, C.; Fujishima, A.; Einaga, Y., High-Yield Electrochemical Production of Formaldehyde from CO2 and Seawater. *Angew. Chem. Int. Ed.* **2014,** *53* (3), 871-874.

(6) Barton, E. E.; Rampulla, D. M.; Bocarsly, A. B., Selective solar-driven reduction of CO_2 to methanol using a catalyzed p-GaP based photoelectrochemical cell. *J. Am. Chem. Soc.* **2008,** *130* (20), 6342-6344.

(7) Jin, D.; Williard, P. G.; Hazari, N.; Bernskoetter, W. H., Effect of Sodium Cation on Metallacycle β-Hydride Elimination in CO_2-Ethylene Coupling to Acrylates. *Chem. Eur. J.* **2014,** *20* (11), 3205-3211.

(8) Kang, P.; Chen, Z.; Brookhart, M.; Meyer, T. J., Electrocatalytic reduction of carbon dioxide: Let the molecules do the work. *Top. Catal.* **2015,** *58* (1), 30-45.

(9) Izumi, Y., Recent advances in the photocatalytic conversion of carbon dioxide to fuels with water and/or hydrogen using solar energy and beyond. *Coordin. Chem. Rev.* **2013,** *257* (1), 171-186.

(10) Inoue, T.; Fujishima, A.; Konishi, S.; Honda, K., Photoelectrocatalytic reduction of carbon dioxide in aqueous suspensions of semiconductor powders. *Nature* **1979,** (227), 637-638.

(11) Yu, J.; Low, J.; Xiao, W.; Zhou, P.; Jaroniec, M., Enhanced photocatalytic CO2-reduction activity of anatase TiO2 by coexposed (001) and (101) facets. *J. Am. Chem. Soc.* **2014,** *136* (25), 8839-8842.

(12) Liao, F.; Huang, Y.; Ge, J.; Zheng, W.; Tedsree, K.; Collier, P.; Hong, X.; Tsang, S. C., Morphology-Dependent Interactions of ZnO with Cu Nanoparticles at the Materials Interface in Selective Hydrogenation of CO2 to CH3OH. *Angew. Chem. Int. Ed.* **2011,** *50* (9), 2162-2165.

(13) Liu, B.-J.; Torimoto, T.; Yoneyama, H., Photocatalytic reduction of CO2 using surface-modified CdS photocatalysts in organic solvents. *Journal of Photochemistry and Photobiology A: Chemistry* **1998,** *113* (1), 93-97.

(14) Costentin, C.; Drouet, S.; Robert, M.; Savéant, J.-M., A local proton source enhances CO_2 electroreduction to CO by a molecular Fe catalyst. *Science* **2012,** *338* (6103), 90-94.

(15) Jitaru, M., Electrochemical carbon dioxide reduction-fundamental and applied topics. *J. Chem. Technol. Metall.* **2007,** *42* (4), 333-344.

(16) Zhang, P.; Wang, M.; Li, C.; Li, X.; Dong, J.; Sun, L., Photochemical H_2 production with noble-metal-free molecular devices comprising a porphyrin photosensitizer and

a cobaloxime catalyst. *ChemComm.* **2010,** *46* (46), 8806-8808.

(17) Hammouche, M.; Lexa, D.; Savéant, J.; Momenteau, M., Catalysis of the electrochemical reduction of carbon dioxide by iron(0) porphyrins. *J. Electroanal. Chem. Interf. Electrochem.* **1988,** *249* (1-2), 347-351.

(18) Smieja, J. M.; Benson, E. E.; Kumar, B.; Grice, K. A.; Seu, C. S.; Miller, A. J.; Mayer, J. M.; Kubiak, C. P., Kinetic and structural studies, origins of selectivity, and interfacial charge transfer in the artificial photosynthesis of CO. *PNAS* **2012,** *109* (39), 15646-15650.

(19) Froehlich, J. D.; Kubiak, C. P., Homogeneous CO_2 reduction by Ni (cyclam) at a glassy carbon electrode. *Inorg. Chem.* **2012,** *51* (7), 3932-3934.

(20) Bourrez, M.; Molton, F.; Chardon-Noblat, S.; Deronzier, A., [Mn (bipyridyl)(CO) $_3$Br]: An abundant metal carbonyl complex as efficient electrocatalyst for CO2 reduction. *Angew. Chem. Int. Ed.* **2011,** *123* (42), 10077-10080.

(21) Hawecker, J.; Lehn, J.-M.; Ziessel, R., Electrocatalytic reduction of carbon dioxide mediated by Re (bipy)(CO) 3 Cl (bipy= 2, 2'-bipyridine). *ChemComm.* **1984,** (6), 328-330.

(22) Benson, E. E.; Kubiak, C. P.; Sathrum, A. J.; Smieja, J. M., Electrocatalytic and homogeneous approaches to conversion of CO_2 to liquid fuels. *Chem. Soc. Rev.* **2009,** *38* (1), 89-99.

(23) Qiao, J.; Liu, Y.; Hong, F.; Zhang, J., A review of catalysts for the electroreduction of carbon dioxide to produce low-carbon fuels. *Chem. Soc. Rev.* **2014,** *43* (2), 631-675.

(24) Chen, Z.; Chen, C.; Weinberg, D. R.; Kang, P.; Concepcion, J. J.; Harrison, D. P.; Brookhart, M. S.; Meyer, T. J., Electrocatalytic reduction of CO_2 to CO by polypyridyl ruthenium complexes. *ChemComm.* **2011,** *47* (47), 12607-12609.

(25) White, T. A.; Maji, S.; Ott, S., Mechanistic insights into electrocatalytic CO_2 reduction within $[Ru^{II}(tpy)(NN)X]^{n+}$ architectures. *Dalton Trans.* **2014,** *43* (40), 15028-15037.

(26) Johnson, B. A.; Maji, S.; Agarwala, H.; White, T. A.; Mijangos, E.; Ott, S., Activating a Low Overpotential CO_2 Reduction Mechanism by a Strategic Ligand Modification on a Ruthenium Polypyridyl Catalyst. *Angew. Chem. Int. Ed.* **2016,** *55* (5), 1825-1829.

(27) Gonell, S.; Massey, M. D.; Moseley, I. P.; Schauer, C. K.; Mucherman, J. T.; Miller, A. J., The *Trans* Effect in Electrocatalytic CO_2 Reduction: Mechanistic Studies of Asymmetric Ruthenium Pyridyl-Carbene Catalysts. *J. Am. Chem. Soc.* **2019,** *141* (16), 6658-6671.